Supplementary Material

Atomistic study of dislocation formation during Ge epitaxy on Si

Luis Martín-Encinar[a,*], Luis A. Marqués[a], Iván Santos[a], Lourdes Pelaz[a]

[a]*Dpto. de Electricidad y Electrónica, E.T.S.I. de Telecomunicación, Universidad de Valladolid, Paseo de Belén 15, 47011, Valladolid, Spain*

S1. Ge-Si intermixing

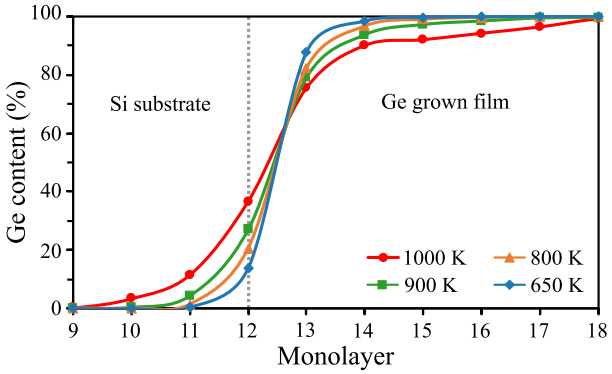

Figure S1: Ge content in each ML around the original position of the Si substrate surface (vertical gray dashed line) after the deposition of 10 Ge MLs at different temperatures. For 650, 800 and 900 K, each data point is the average of the five simulated cases shown in Table 1 of main text (dispersion in the Ge content values is negligible, so we omitted the error bars for clarity). At these temperatures, no dislocations have been formed yet, as the critical thickness is above 10 MLs (see Fig. S2). For 1000 K, data points correspond to one particular case where a dislocation formed in order to illustrate its role in intermixing.

*Corresponding author
Email address: luis.martin.encinar@uva.es (Luis Martín-Encinar)

S2. Critical thickness

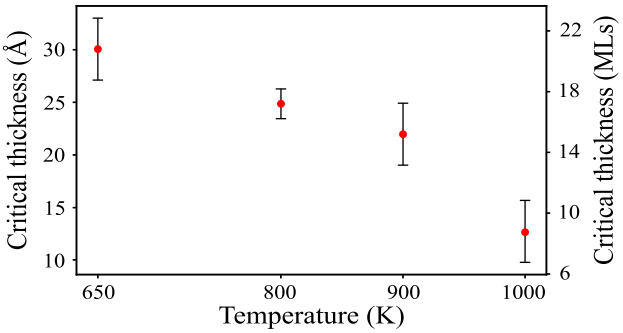

Figure S2: Average critical thickness extracted from the simulations of Table 1 (main text). For each point, error bars display the standard deviation.

S3. Stress relaxation

The average biaxial stress per layer l, S_l^{biax} is calculated as:

$$S_l^{biax} = \frac{\sum_i \left(S_{i,l}^{xx} + S_{i,l}^{yy}\right)}{2N^l}, \tag{1}$$

where N^l is the number of atoms in layer l and $S_{i,l}^{xx}$ ($S_{i,l}^{yy}$) is the xx (yy) component of the atomic stress for i-atoms belonging to layer l. The normal stress component $S_{i,l}^{zz}$ is negligible as the system is free to expand along the Z direction. Stress is positive for tension and negative for compression.

Figure S3.1 compares the biaxial stress per ML at different temperatures once the deposition process is completed. The reduction in compressive stress in the Ge grown film depends on the formed dislocation network. For instance, the dislocation network observed at 1000 K (60°/90° MDs in the Y direction and a Frank PD along the X direction, both reaching the Si/Ge interface) releases twice the stress compared to the dislocation network formed at 800 K (two 60° MDs connected by PBC that lie at the interface). The fact that dislocations reach the Si/Ge interface is crucial for stress relaxation. In the simulation at 650 K, an incipient dislocation has only propagated in the top half of the Ge grown film (up to the 32$^{\text{nd}}$ ML), and the biaxial stress underneath is very similar to the reference value. The small release of stress between 15$^{\text{th}}$ and 30$^{\text{th}}$ MLs is due to intermixing (negligible contribution compared to the strain released by dislocations).

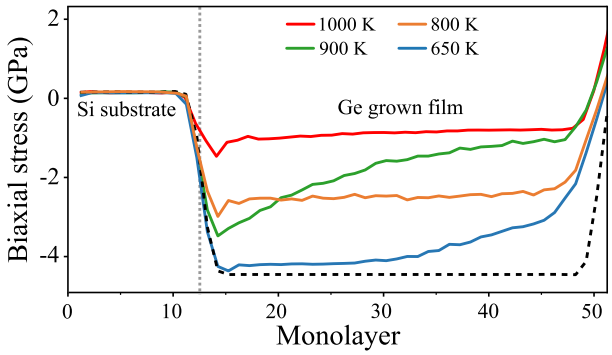

Figure S3.1: Distribution of the average biaxial stress per ML for the cases of Fig. 2 (main text) once deposition process is completed. The dashed black line denotes the biaxial stress of 40 Ge strained MLs coherently grown on 12 Si MLs. The vertical gray dashed line indicates the position of the original Si substrate surface. In the Si substrate region, the atoms are placed in relaxed lattice positions, thus the average biaxial stress is nearly zero. In the Si/Ge interface region, the biaxial stress shows an abrupt transition with a sharp drop to negative values (compressive stress), evidencing the lattice mismatch between Ge and Si. In the Ge grown film region above the Si/Ge interface, the biaxial stress per ML is related to the amount, type, size and arrangement of the formed dislocations in each case. From the 46$^{\text{th}}$ ML onward, the reduction of the compressive biaxial stress and even the transition to tensile indicate the proximity of the surface. Values of the biaxial stress are not fully meaningful here due to the approximate calculation of V_i for surface atoms.

To illustrate the role of 90° MDs, we have selected those simulations of Table 1 (main text) with isolated straight 90° MDs and combinations of them. Figure S3.2 plots the biaxial

stress per ML for the simulated cases with one or two perpendicular 90° MDs, either reaching the interface or not.

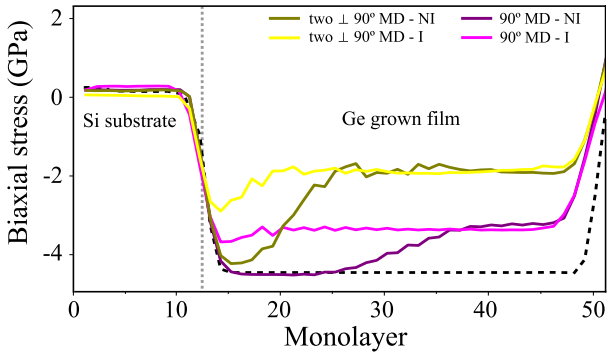

Figure S3.2: Distribution of the average biaxial stress per ML in samples where different 90° MDs were formed. The dashed black line denotes the biaxial stress of 40 Ge strained MLs coherently grown on 12 Si MLs. Abbreviations I and NI indicate if the dislocation line reaches the interface or not, respectively. The vertical gray dashed line shows the position of the original Si substrate surface.

The formation of a single 90° MD that reaches the interface either in X or Y direction (magenta line) releases approximately 1.3 GPa ($\sim$ 30%) of the biaxial stress in each layer above the dislocation line. Two perpendicular 90° MDs that also reach the interface (yellow line) release approximately 2.7 GPa ($\sim$ 60%) of the biaxial stress in each layer above the dislocations lines, which is double the value compared to a single 90° MD. This result is in agreement with theory since as our cell size along X and Y directions is $\sim$ 18 nm, the degree of relaxation in the presence of a 90° MD in each direction (i.e. two orthogonal 90° MD) at the interface should correspond to a $\sim$ 65% relaxation of the $\sim$4% Ge/Si lattice mismatch [14].

In both cases, either involving a single 90° MD or two perpendicular 90° MDs, if the dislocation does not reach the Si/Ge interface (dark purple or olive lines), the stress under the dislocation is high, and the transition from non-relaxed to relaxed stress regions occurs gradually. The extent of this transition is influenced by whether the dislocation line is straight or exhibits irregularities such as jogs or kinks.

S4. Dislocation multiplication

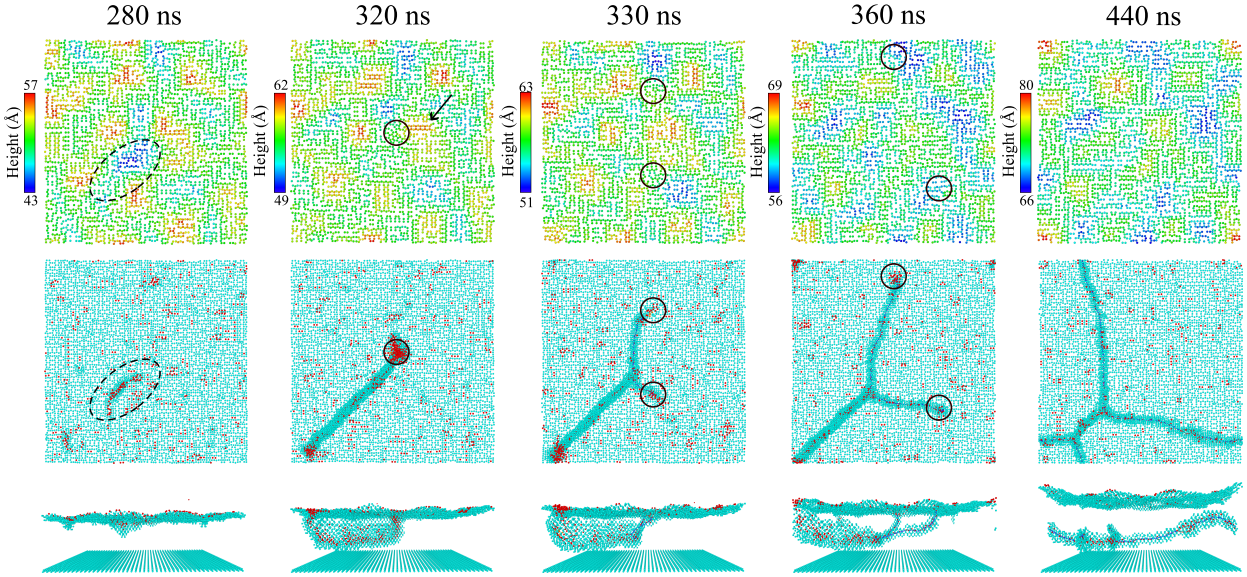

Figure S4: Sample snapshots taken at different times during one of the deposition simulations carried at 1000 K. Upper panels are top views where atoms are colored according to their height. Middle panels are also top views where atoms are colored according to their local structure: cubic diamond up to 1st or 2nd neighbors (■), hexagonal diamond (■), and *other* (■) (perfect cubic diamond atoms are not shown). Bottom panels are perspective views of atoms shown in middle panels. Dashed ovals indicate the valley and disordered region where the dislocation starts to form. Full circles highlight the position of dislocation threading arm ends. Dark blue lines are dislocation lines as identified by OVITO. During its propagation, one of the ends of the dislocation half-loop finds a surface island (pointed by the arrow). To avoid it, the dislocation splits in two (dislocation multiplication).

S5. Post-growth annealing of a 90° MD

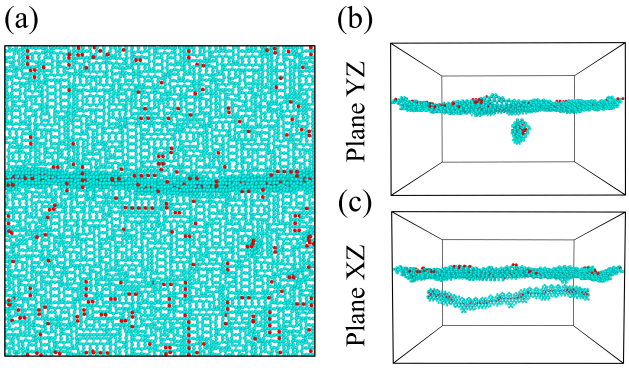

Figure S5: Snapshots taken after a 40 ns annealing at 900 K of the last sample shown in Fig. 4 (main text). (a) is a top view, while (b) and (c) are perspective views. Atoms are colored according to their local structure: cubic diamond up to 1^{st} or 2^{nd} neighbors (■), and *other* (■) (perfect cubic diamond atoms are not shown). After annealing, the dislocation line is straight in plane XZ as kinks have been eliminated.

S6. Stress relaxation during dislocation formation

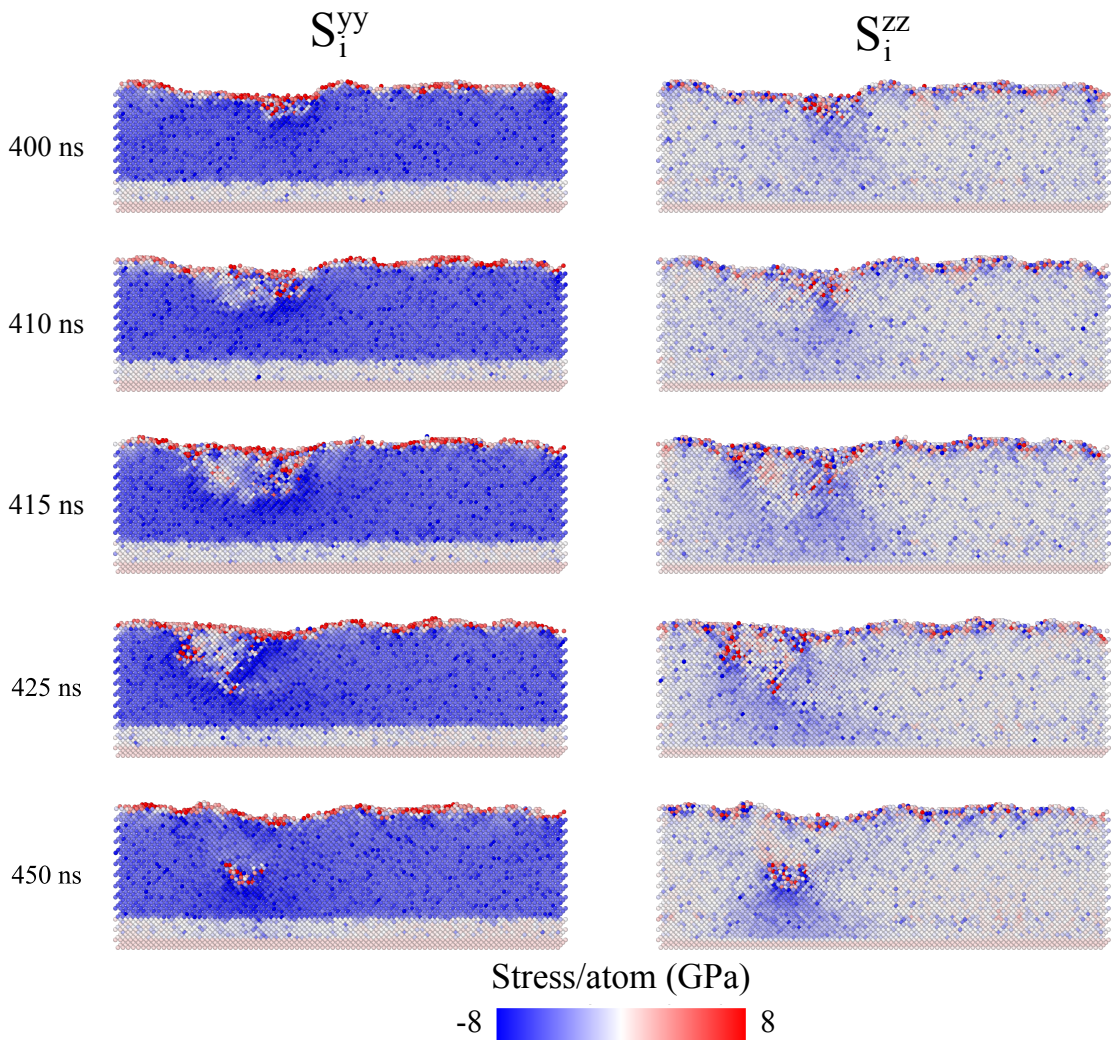

Figure S6: Snapshots showing atoms within a 17 Å slice in the (100) plane around the disordered region whose evolution was shown in Fig. 4 (main text). Atoms are colored according to the yy (left) and zz (right) components of the atomic stress tensor (blue means compressive and red tensile). The behavior of the yy component shows a compressed film which is more relaxed in the disordered region and has a higher compression under it, similar to the one obtained for the xx component shown in Fig. 5 (main text). Differences with respect to the xx component are evidenced from t=415 ns as the dislocation half-loop formed and propagated mainly on the Y direction, which causes stress relaxation in the xx component but not in the yy component. For the zz component, the Ge film appears relaxed since the simulation cell has free boundary conditions along Z and, consequently, the Ge film naturally relaxes along that direction as deposition proceeds. Only a small compression is observed under the disorder region and the dislocation.

S7. Dislocation nucleation and propagation during deposition using the Tersoff potential

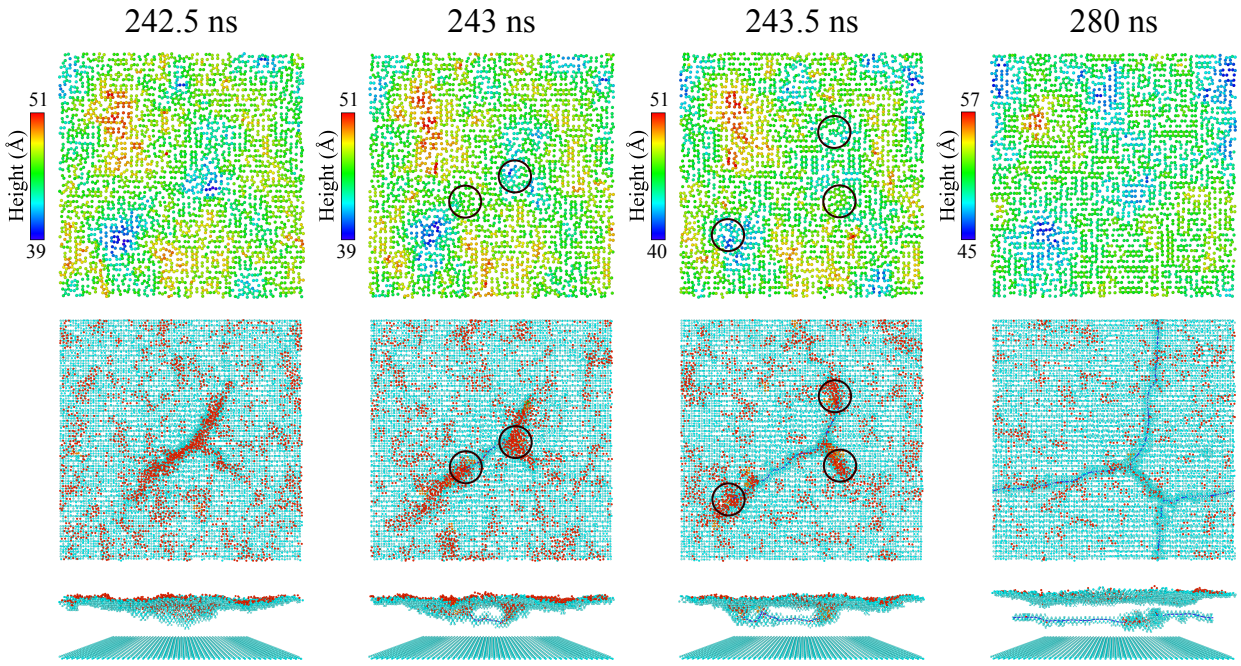

Figure S7: Sample snapshots taken at different times during a deposition simulation carried at 2000 K using the Tersoff potential (J. Tersoff, Phys. Rev. B 39, 1989, p. 5566). Upper panels are top views where atoms are colored according to their height. Middle panels are also top views where atoms are colored according to their local structure: cubic diamond up to 1st or 2nd neighbors (■), hexagonal diamond (■), and *other* (■) (perfect cubic diamond atoms are not shown). Bottom panels are perspective views of atoms shown in middle panels. Full circles highlight the position of dislocation threading arm ends. Dark blue lines are dislocation lines as identified by OVITO. The processes of formation and propagation of dislocations are the same as with the SW potential: generation and growth of an amorphous region from a surface valley (t=242.5 ns), its partial recrystallization giving rise to a dislocation half-loop (t=243 ns), the propagation of its threading arm ends (which keep their amorphous nature) along the surface avoiding islands (t=243.5 ns), until the generation of the final dislocation network (t=280 ns), which in this case consists of two perpendicular 90° MDs (multiplication mechanism similar to the one shown in Fig. S4). Considering this and other test simulations with the Tersoff potential, the only differences found with respect to the SW potential simulations are that final dislocation cores show less point defects and that SFs are more frequent.